scientific reports

Check for updates

OPEN

CCR7 depletion alleviates bony growth imbalance following physeal injury in mice

WooYoung Kim[1,2], Yuko Sakai[1,2], Masatake Matsuoka[1]✉, Yoshiaki Hosokawa[1], Ryuichi Fukuda[1], Kentaro Homan[1], Tomohiro Onodera[1] & Norimasa Iwasaki[1]

Growth plates are the frequent sites of skeletal injury in children, leading to skeletal growth imbalances. Chemokines, including the receptor CCR7, play a crucial role in stem cell recruitment and cartilage homeostasis, with previous studies linking CCR7 to osteoarthritis progression. However, its role in growth plate cartilage remains unclear. We analyzed the role of CCR7 in the physeal cartilage repair process in mice model. Physeal injury was created in the proximal tibia in 3-week-old C57BL/6 mice (WT) and CCR7-knockout mice (CCR7−/−). Tibial length was measured macroscopically and sections of the physeal injury were analyzed histologically and immunohistochemically. Height and bone volume of the tibial growth plate and bone mineral density (BMD) of the subchondral area were measured by micro-CT. Mesenchymal stem cells (MSCs) were harvested and gene expression after osteogenic differentiation was analyzed using qRT-PCR. At 1, 3 and 5 weeks postoperatively, injured tibiae of CCR7−/− mice were less shortened than those of WT mice. Bone volume of the physeal bridge was significantly lower in CCR7−/− mice than in WT mice. In contrast, BMD of the subchondral area was comparable between CCR−/− and WT mice, and between sham and operated tibiae. In osteogenic differentiation, CCR7−/− mice showed significantly lowered expression of osteogenic markers such as Osterix, Runx2 and Type X collagen. We demonstrated CCR7 depletion in mice inhibited physeal bridge formation and ameliorated growth imbalances after physeal injury.

Physeal injury constitutes 30% of pediatric bone fractures and 10% of such injuries cause shortening or deformation of the limbs, resulting in severe social and economic problems[1,2]. Bony growth along the longitudinal axis is usually controlled by vascular invasion following hypertrophy of chondrocytes in the growth plates of the long bones[3]. Physeal injury causes partial ossification of chondrocytes in the injured plate, burdening the young individual with disturbance of bone growth. However, the precise mechanisms involved remain unclear.

Current therapeutic techniques to address physeal arrest involve bony bar resection and interpositional materials such as fat or silicone rubber to prevent reformation of bony tissue and allow the intact physeal cartilage to restore normal growth. However, clinical success rates following resection range from 18–35%[4]. In addition, fat grafts do not integrate into host tissue but instead break down over time, leading to physeal closure or bony bar recurrence. Silicone rubber does not incorporate within host tissues and may migrate from the surgical site, causing subsequent problems. The capricious nature of invasive surgery with the interposition of imperfect graft materials therefore results in high rates of bar reformation, speaking to the critical need for novel, regenerative treatment methods[2].

Chemokines are low molecular weight proteins of 8–10 kDa and are known to play a crucial role in recruiting stem cells or precursor cells. Previous reports demonstrated, through comprehensive chemokine screening, that the chemokine receptor CCR7 is most important for maintaining articular cartilage homeostasis[5]. Additionally, CCR7 has been observed in knee osteoarthritis and is associated with the severity of symptoms. Furthermore, CCR7-deficient mice showed delayed development of joint damage and functional deficits in a murine model of osteoarthritis[6]. However, the roles of CCR7 in growth plate cartilage remain unclear.

Based on previous studies, we hypothesized that CCR7 play a critical role in bony growth during physeal injury and the repair process. To this end, we employed CCR7-knockout mice to analyze the role of CCR7 in the process of growth plate cartilage repair.

[1]Department of Orthopaedic Surgery, Faculty of Medicine, Graduate School of Medicine, Hokkaido University, North-15 West-7, Kita-Ku, Sapporo, Hokkaido 060-8638, Japan. [2]WooYoung Kim and Yuko Sakai contributed equally. ✉email: masatakem@pop.med.hokudai.ac.jp

Results

CCR7 is expressed at the injury site immediately after physeal injury

We first analyzed CCR7 expression 1 day after physeal injury created in the proximal tibia in mice model. CCR7 accumulated predominantly at the injury site and was barely expressed in the remaining physeal chondrocytes (Fig. 1). In addition, VEGF, as a marker of osteoprogenitor cells, was also expressed in the same areas where CCR7 was found to be expressed. Further expression analysis revealed the presence of CD44, Type I, and Type X collagen-positive cells at the injury site (Supplemental Fig. 1). These results suggest that osteoprogenitor cells are recruited by CCR7 and express VEGF. Accordingly, CCR7−/− mice were employed in the following experiments.

CCR7 deficiency suppresses shortening of bony length after physeal injury

No significant difference in uninjured tibial length and was observed between 3-week-old WT mice and CCR7−/− mice (Supplemental Fig. 2A). At 1, 3, and 5 weeks postoperatively, both injured and intact tibiae from the same mouse were harvested and subjected to analysis. Macroscopic findings showed that the injured tibia was shortened in WT mice, whereas in CCR7−/− mice, the length of the injured tibia was comparable to that on the control side (Fig. 2A). Tibial length in WT mice was significantly shorter compared to the sham-operated tibia following growth plate injury (mean ± standard deviation: 13.24 ± 0.25 mm in the operated tibia vs. 13.58 ± 0.25 mm in the sham group at 1 week, $p < 0.01$; 15.13 ± 0.25 mm in the operated tibia vs. 15.56 ± 0.29 mm in the sham group at 3 weeks, $p < 0.01$; 15.65 ± 0.35 mm in the operated tibia vs. 16.05 ± 0.31 mm in the sham group at 5 weeks, $p = 0.02$; Fig. 2B). In contrast, no significant differences in tibial length were observed between the operated and sham-operated tibiae following growth plate injury in CCR7−/− mice (13.39 ± 0.32 mm in the operated tibia vs. 13.44 ± 0.31 mm in the sham group at 1 week, $p = 0.72$; 15.29 ± 0.37 mm in the operated tibia vs. 15.42 ± 0.32 mm in the sham group at 3 weeks, $p = 0.43$; 15.76 ± 0.65 mm in the operated tibia vs. 15.93 ± 0.59 mm in the sham group at 5 weeks, $p = 0.57$; Fig. 2B). These results suggested that depletion of CCR7 inhibited the shortening of longitudinal bone growth after physeal injury.

Micro-CT evaluation and histology: CCR7 deficiency shows hindered formation of the physeal bridge

Next, we examined whether CCR7 deficiency influenced physeal bridge formation using micro-CT. Bone volume of the physeal bridge was significantly lower in CCR7−/− mice than in WT mice at 1, 3 and 5 weeks (143.00 ± 3.09 Hounsfield units (HU) in WT vs. 138.95 ± 1.58 HU in CCR7−/− at 1 week, $p < 0.05$; 143.16 ± 9.21 HU in WT vs. 130.37 ± 7.62 HU in CCR7−/− at 3 weeks, $p < 0.01$; 150.29 ± 4.59 HU in WT vs. 142.84 ± 5.07 HU in CCR7−/− at 5 weeks, $p < 0.01$; Fig. 3A and B). Although no difference in growth plate height and morphology

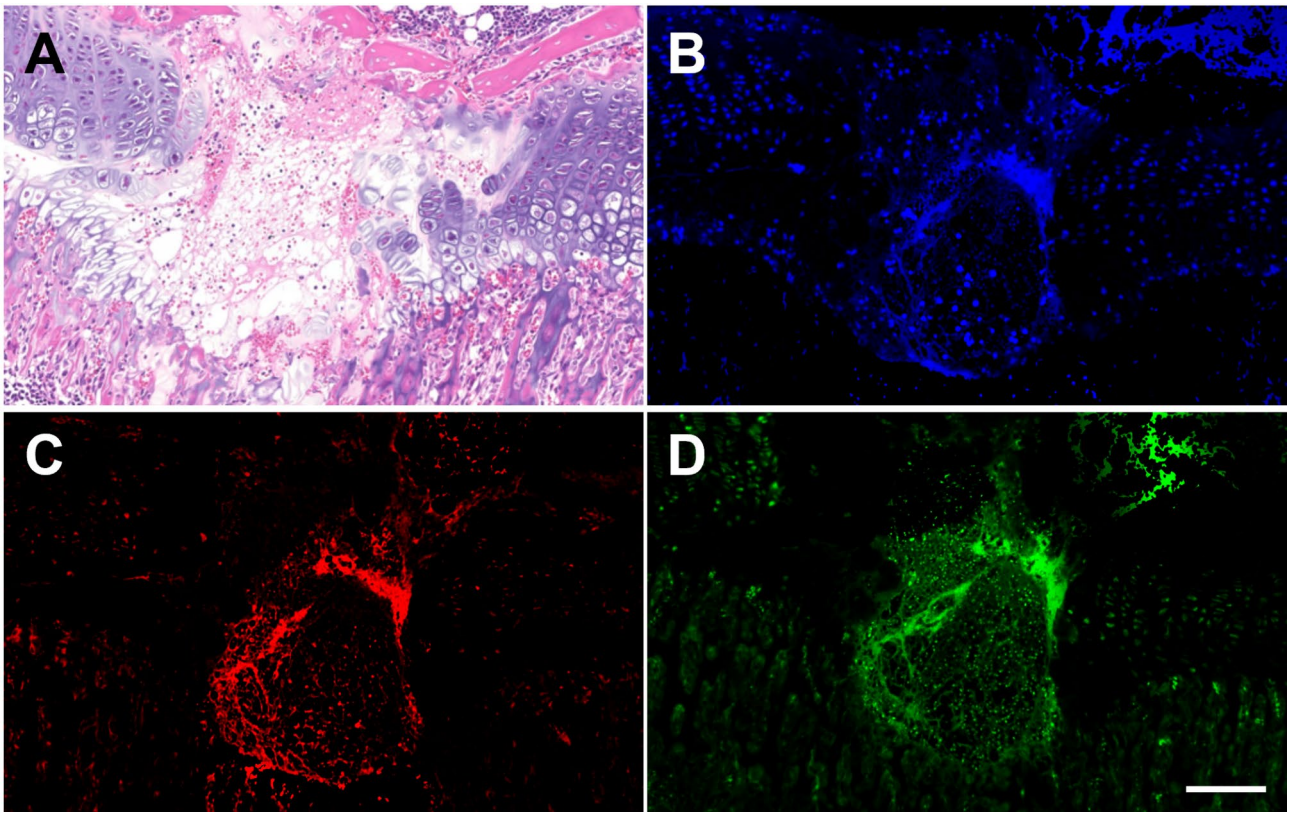

Fig. 1. Histological analysis at 1 day postoperatively. **A** HE staining. **B** DAPI staining. **C** CCR7. **D** VEGF. Scale bar: 0.2 mm.

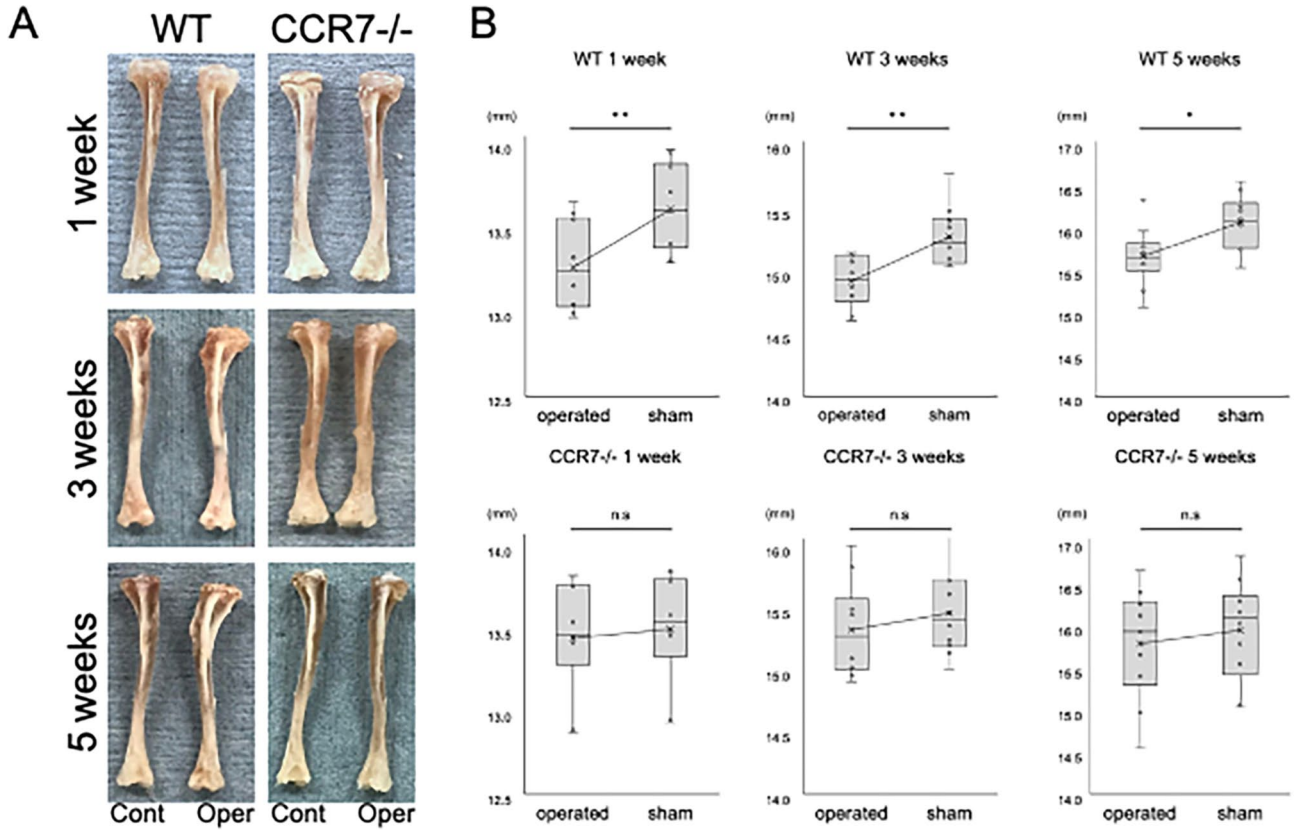

Fig. 2. Macroscopic observations of tibiae after physeal injury ($n = 10$/group). **A** Real image of wild-type (WT) and CCR7−/− mice. **B** Comparison of tibial length after physeal injury. Cont: control; Oper: operated; WT: wild-type; CCR7−/−: CCR7 knockout. Values represent mean ± standard deviation. *,**Significance at the level of $P < 0.05$ and $P < 0.01$, respectively. n.s: no significance.

were observed between 3-week-old WT and CCR7−/− mice (Supplemental Fig. 2B-D), in WT mice, a significant change in growth plate height was observed at 3 and 5 weeks postoperatively (0.21 ± 0.019 mm in the operated tibia vs. 0.22 ± 0.015 mm in the sham group at 1 week, $p = 0.53$; 0.16 ± 0.019 mm in the operated tibia vs. 0.19 ± 0.030 mm in the sham group at 3 weeks, $p < 0.01$; 0.12 ± 0.13 mm in the operated tibia vs. 0.15 ± 0.022 mm in the sham group at 5 weeks, $p < 0.01$, Fig. 3C). In contrast, no significant changes were observed after growth plate injury in CCR−/− mice (0.20 ± 0.023 mm in the operated tibia vs. 0.19 ± 0.021 mm in the sham group at 1 week, $p = 0.34$; 0.14 ± 0.020 mm in the operated tibia vs. 0.14 ± 0.019 mm in the sham group at 3 weeks, $p = 0.84$; 0.14 ± 0.020 mm in the operated tibia vs. 0.14 ± 0.019 mm in the sham group at 5 weeks, $p = 0.44$, Fig. 3C). In contrast, BMD of the subchondral area was comparable between WT and CCR−/− mice, and between sham and operated tibia at all time points (0.412 ± 0.09% in control WT mice vs. 0.442 ± 0.12% in operated WT mice at 1 week, $p = 0.42$; 0.433 ± 0.08% in control CCR−/− mice vs. 0.422 ± 0.15% in operated CCR−/− mice at 1 week, $p = 0.58$; 0.468 ± 0.05% in control WT mice vs. 0.426 ± 0.06% in operated WT mice at 3 weeks, $p = 0.68$; 0.467 ± 0.04% in control CCR−/− mice vs. 0.411 ± 0.09% in operated CCR−/− mice at 3 weeks, $p = 0.12$; 0.441 ± 0.07% in control WT mice vs. 0.396 ± 0.06% in operated WT mice at 5 weeks, $p = 0.49$; 0.466 ± 0.05% in control CCR−/− mice vs. 0.424 ± 0.07% in operated CCR−/− mice at 5 weeks, $p = 0.72$; Fig. 3D).

HE staining showed differences in physeal bridge formation at the injury site. WT mice showed a denser, more continuous bony bar with less infiltration of bone marrow, cavities or disconnection starting to form at 1 week (Fig. 4A–C), while the physeal bridge in the CCR7−/− mice showed a rather sparse, unstable and discontinuous shape, partly empty, especially at 5 weeks (Fig. 4D–F). Moreover, in WT mice, VEGF-expressing cells were observed up to 1 week postoperatively (Fig. 4G–I). In contrast, in CCR7-deficient mice, VEGF-expressing cells were hardly detected at 1 week postoperatively (Fig. 4J–L). Combined with the results from micro-CT analysis, these results suggested that CCR7 deficiency suppressed the induction of ossification at the site of physeal injury.

Depletion of chemokine CCR7 suppresses osteogenic differentiation

To further assess the effects of CCR7 deficiency on osteogenicity, we performed osteogenic differentiation. After 14 days of cultivation in differentiation medium, MSCs of CCR7−/− showed significantly lowered expressions of ossification markers such as Osterix, Runt-related Transcription Factor 2 (Runx2) and Type X collagen (Col X) (OPN: 1.00 ± 0.16 in WT vs. 0.88 ± 0.14 in CCR−/−, $p = 0.28$; Osterix: 1.02 ± 0.22 in WT vs. 0.78 ± 0.05 in CCR−/−, $p = 0.03$; Runx2: 1.01 ± 0.16 in WT vs. 0.63 ± 0.12 in CCR−/−, $p = 0.01$; BMP-2 : 1.01 ± 0.17 in WT vs. 0.91 ± 0.11 in CCR−/−, $p = 0.39$; Col X : 1.05 ± 0.16 in WT vs. 0.7 ± 0.04 in CCR−/−, $p = 0.02$; VEGF: 1.01 ± 0.19

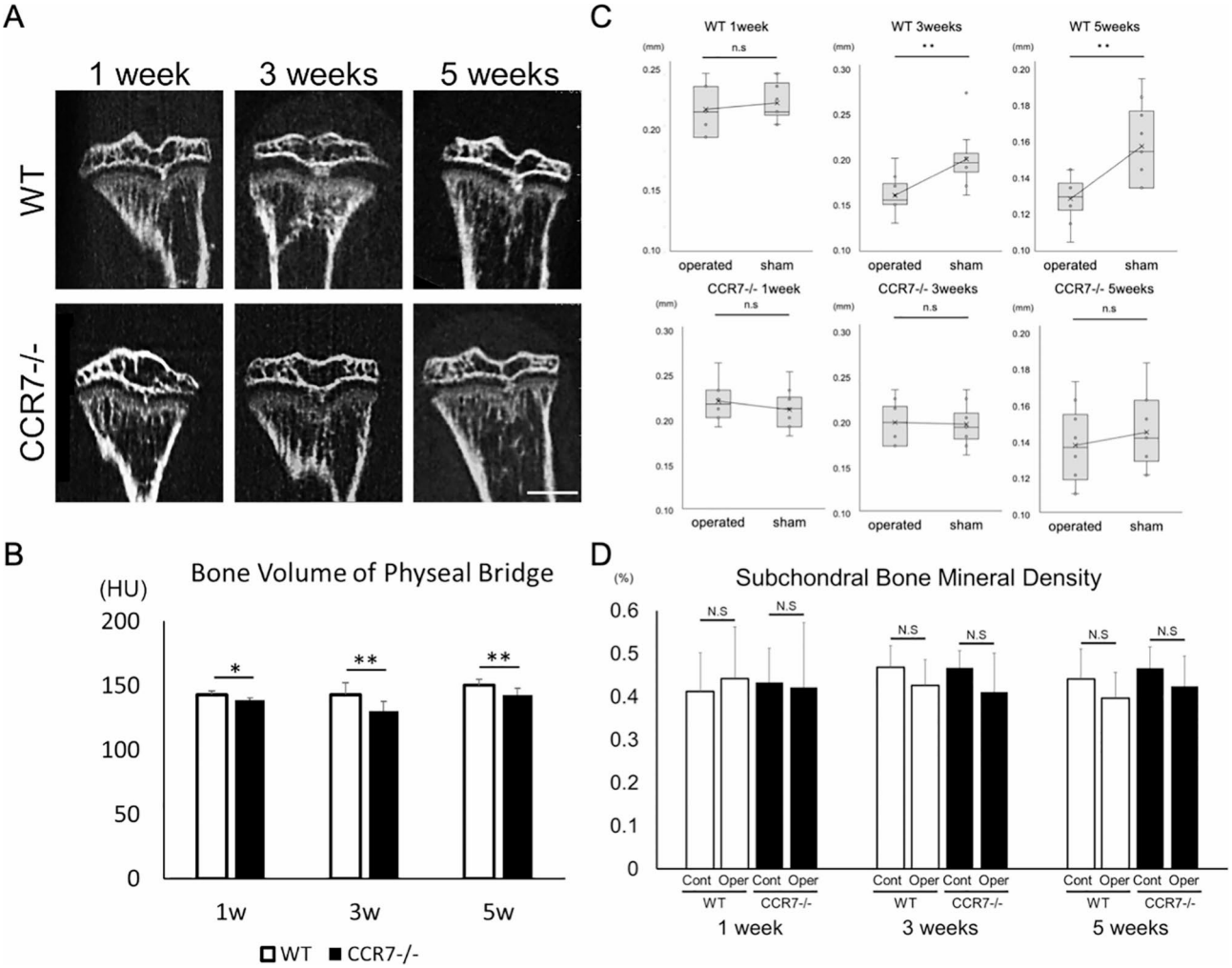

Fig. 3. Micro-CT analysis ($n = 10$/group). **A** Micro-CT images showing bony bar formation within the physeal injury site. **B** Bone volume of the bony bar. **C** Comparison of growth plate height between WT and CCR7−/−. **D** Subchondral bone mineral density. Scale bar: 1 mm. Cont: control; Oper: operated; WT: wild-type; CCR7−/−: CCR7-knockout. Values represent mean ± standard deviation. *,**Significance at the level of $P < 0.05$ and $P < 0.01$, respectively. n.s: no significance.

in WT vs. 1.04 ± 0.27 in CCR−/−, $p = 0.92$; Fig. 5). Alizarin red staining showed that the staining intensity in CCR7−/− mice was reduced compared to WT mice (Fig. 5G and H). These results indicate that CCR7 not only facilitates the recruitment of osteoprogenitor cells to the injury site after growth plate injury but also plays a promotive role in osteogenesis.

Discussion

Using comprehensive screening techniques, including differences in tibia length, micro-CT analysis, histology and immunohistochemistry, as well as osteogenic differentiation from MSCs, we identified chemokine receptor CCR7 as a candidate therapeutic target involved in the repair process after physeal injury. CCR7 is involved in multiple pathophysiological processes, including inflammation and tumorigenesis[7,8]. However, the roles of CCR7 in musculoskeletal diseases have rarely been addressed[5,6]. The present study demonstrated that CCR7 knockout in mice inhibited physeal bridge formation and ameliorated growth imbalances after physeal injury with sparse and discontinuous bony bar on histology, and decreased bone volume on micro-CT. Based on the current results, CCR7 appears to play crucial roles in bony physeal bridge formation. However, the molecular mechanisms involved are still unclear.

In our analysis, VEGF-expressing osteoprogenitor cells co-expressed CCR7 immediately after physeal injury. In addition, MSCs during osteogenesis in CCR7−/− mice showed reduced gene expressions of osteogenic markers in qRT-PCR, implying that close relations exist among CCR7 and osteogenesis. As aforementioned, the chemokine receptor CCR7 has been mainly studied in the field of immunology and oncology due to its role in the migration of inflammatory cells and the metastasis of cancer cells[9–13]. Of note, some of those studies addressed the relationship between CCR7 activation and VEGF expression. More precisely, they showed that

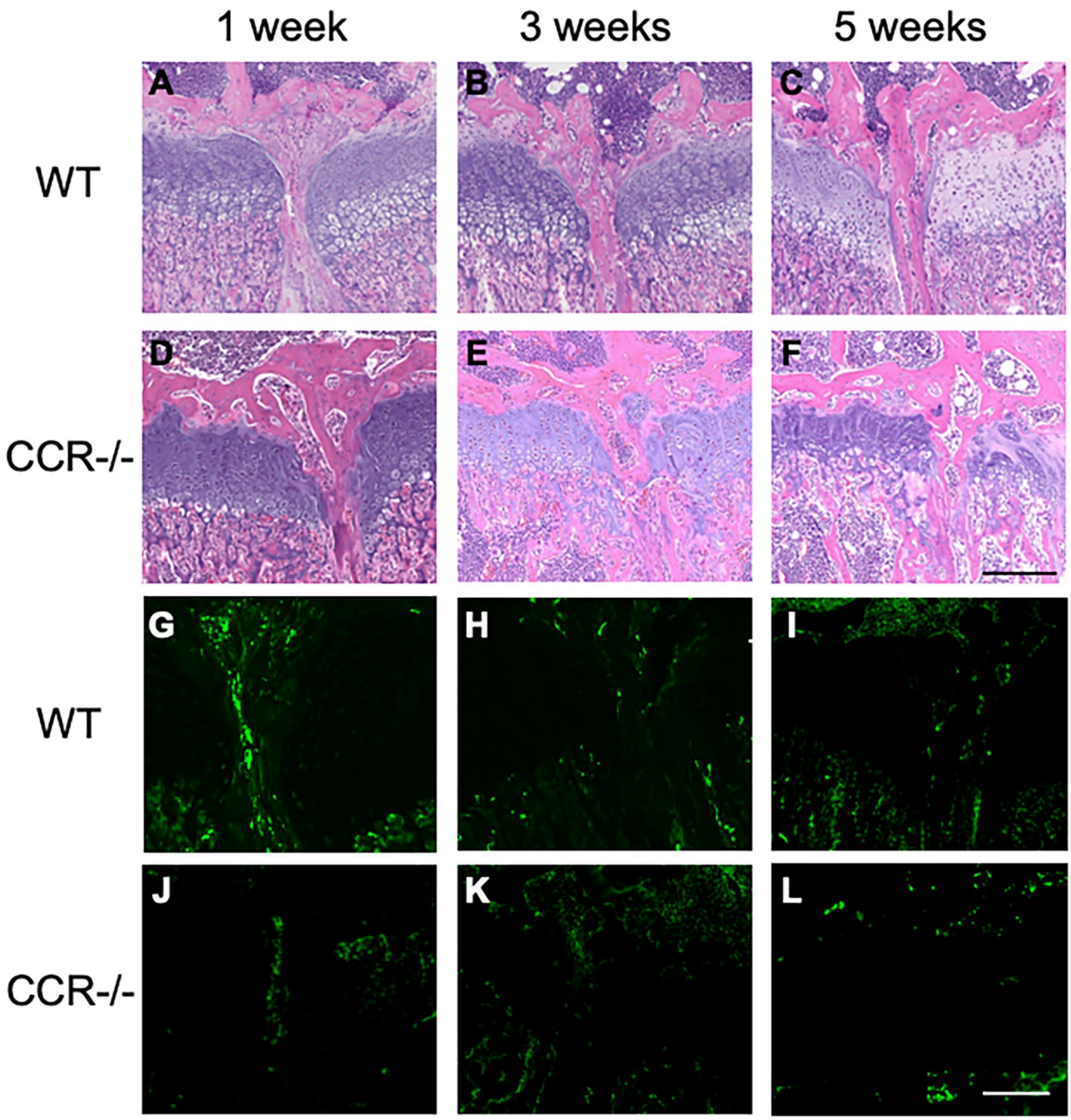

Fig. 4. Histology of physeal bridge formation at different time points after injury. Hematoxylin and eosin staining (**A**–**F**) and VEGF (**G**–**L**). Histology shows differences in bony proportion of the physeal bridge in the presence (**A**–**C** and **G**–**I**) or absence (**D**–**F** and **J**–**L**) of CCR7. Scale bar = 0.2 mm. WT: wild-type; CCR7−/−: CCR7 knockout.

CCR7 activation induced VEGF expression via MAPK or NF-κB pathways[14–16]. Interestingly, those reports also support the molecular pattern identified during physeal injury and repair in our study.

Hypoplasia of the bony bar at physeal injury in CCR7−/− mice may primarily result from suppression of osteogenic differentiation. Because a high VEGF level during late-stage chondrogenesis is known to promote endochondral ossification to convert hypertrophic cartilage into bone[17], the suppression of angiogenesis by lower expression of VEGF could suppress the conversion of cartilage into bone at the site of growth plate injury. Similarly, Chung et al. reported that systemic anti-VEGF treatment inhibited physeal bridge formation, causing short stature in a rat model of physeal injury[18]. Meanwhile, Erickson et al. reported the local anti-VEGF treatment inhibited physeal bridge formation, with no effect on limb lengthening[19]. However, our study model using systemic CCR7−/− in mice did not result in growth impairment or differences in the BMD at the subchondral area. Our previous study also showed no growth difference between WT and CCR7−/− mice[5].

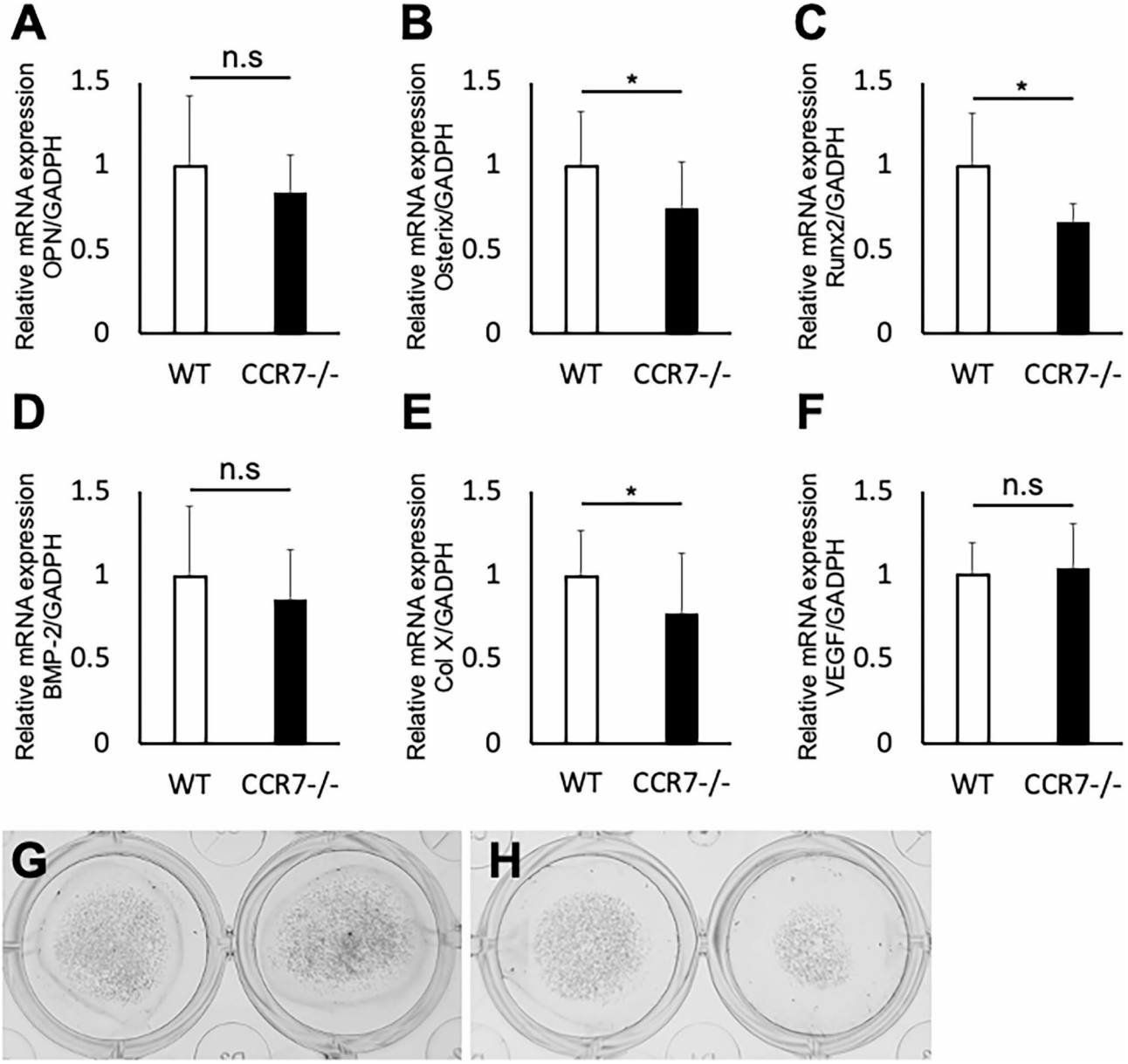

Fig. 5. Gene expression of MSCs during osteogenic differentiation as analyzed by quantitative real-time polymerase chain reaction (**A**–**F**) and alizarin red staining (**G** WT, **H** CCR7−/−). WT: wild-type; CCR7−/−: CCR7-knockout. Values represent mean ± standard deviation ($n = 6$). *Significance at the level of $P < 0.05$. n.s: no significance.

Putting these results together, the present study suggests that CCR7 induced VEGF expression at the injury site in a limited manner, exerting little influence on growth in the normal state. Systemic therapy via CCR7 may thus be non-invasive and represents an avenue for future investigations of therapy after physeal injury.

Some limitations should be considered when interpreting our results. First, in this study, the viability of remnant physeal cartilage after physeal injury was unclear. Expression of CCR7 is more concentrated in injured than in non-injured areas, and the role of CCR7 after physeal injury presumably mainly involves bone bridge formation in the injured area, but the exact roles in non-injured areas need to be clarified in future studies. Second, although we demonstrated that depletion of CCR7 suppressed osteogenesis, the mechanisms by which CCR7 regulates osteogenic gene expression at the injury site remain unclear. Finally, since this study used a mouse model, human samples need to be analyzed in the future. Nonetheless, this represents the first study to investigate the relationship between CCR7 and repair of physeal injury and will provide a foundation for future treatment strategies to inhibit physeal bridge formation after physeal injury.

In summary, we demonstrated depletion of CCR7 ameliorated growth imbalances after physeal injury in a mouse model, suggesting the possibility of suppressing expression of ossification markers. Strategies to inhibit physeal bridge formation by manipulating CCR7 may be a future direction for treating physeal injury.

Methods

Experimental animals

All experiments were performed according to a protocol approved by the Institutional Animal Care and Use Committee of the Hokkaido University Graduate School of Medicine. CCR7-knockout mice (CCR7−/−) were obtained from The Jackson Laboratory (strain B6, 129P2(C)–Ccr7tm1Rfor/J, stock number 006621). C57BL/6 mice were purchased from Japan SLC, Inc. and used as wild-type (WT) mice. Mice were housed in a temperature- and humidity-controlled environment under 12-h light/12-h dark conditions and fed a standard rodent diet in accordance with our institutional guidelines for the care and use of laboratory animals. Scorings were performed independently by two blinded observers.

Operative procedure for physeal cartilage injury in mice

Full-thickness physeal injuries were generated in 3-week-old female WT and CCR7−/− mice for consistency with a previous study[20] ($n=10$/group). The injury group comprised physeal injuries created in the left knee, while the control group comprised sham operation in the right knee of the same mice. Under general anesthesia, hind limbs were disinfected. A medial parapatellar incision slightly less than 0.5 cm in length was then made using a microsurgical scalpel, rendering the tibiae visible. The proximal tibial growth plate was entirely pierced in a lateral-medial direction using a 25-G needle[20]. These microsurgical procedures were performed under a surgical microscope (SZX16; Olympus, Tokyo, Japan). After irrigation with normal saline to remove debris, the skin was sutured in separate layers. Postoperatively, mice were warmed until recovery from anesthesia was confirmed. Tibiae were harvested and analyzed at 1 day, or 1, 3 or 5 weeks postoperatively.

Macroscopic evaluation

Both tibiae of each mouse were harvested at 1, 3 or 5 weeks postoperatively ($n=10$ each). The entire tibia was carefully detached then collected and photographed with a millimeter-scale marker before fixation in formalin for histological analysis. The length of the tibia from the inferior articular surface to the tibial plateau was measured macroscopically using Image J software (version 1.53c; National Institutes of Health).

Micro-computed tomography (micro-CT) analysis

Micro-CT was used to quantify bony bar formation within the injured physis, bone mineral density (BMD) of the subchondral area and growth plate height. Tibiae underwent micro-CT (70 kVp; 200 µA; integration time, 300 ms) for a 15.6-µm isotropic voxel size (VivaCT80; Scanco). A volume of interest (VOI) was drawn by manually outlining a standardized 2.5 mm wide × 160 slice (~2.5 mm) deep area within the physis in the sagittal plane, capturing the entire bony bar that formed within the injured physis. These image stacks were thresholded globally and bony bar formation within the injury was measured and reported as bone volume/total volume (BV/TV). BMD of the subchondral area 40 slices below the growth plate was measured. The regions of interest were manually set at the cylindrical defect area (5.0 mm in diameter). The threshold levels of gray values (covered less than 50% of total sectioned area) were set uniformly for all samples. Both parameters were calculated using the BoneJ plugin with ImageJ software (version 1.53c; National Institutes of Health).

Histological processing

At each time point, tibiae were disarticulated and fixed in 10% formalin (Wako, Tokyo, Japan), then decalcified with ethylenediaminetetraacetic acid (EDTA). When sections were embedded in paraffin, the tibial axis was carefully adjusted to be upright against the surface embedding, and midsagittal sections were then created at 5-mm intervals and stained with hematoxylin and eosin (HE). In addition, for tibiae at 1 day postoperatively, sections were incubated with primary antibodies for CCR7 (Abcam), vascular endothelial growth factor (VEGF) (R&D), CD44 (BD bioscience), Type I collagen (XX) and Type X collagen (XX). Staining was visualized with Alexa Fluor plus 594 (A32740; Invitrogen) for CCR7, FITC Conjugated AffiniPure (Jackson ImmunoResearch) for VEGF and DAB (diaminobenzidine) for CD44, Type I collagen (Sigma-Aldrich) and Type X collagen (LSL). Nuclei were stained using DAPI (Invitrogen).

Mesenchymal stem cell (MSC) culture and osteogenic differentiation

MSCs were harvested and cultured as previously reported[21,22]. Briefly, the humerus, femur and tibia of a 2- to 3-week-old mouse were harvested, with epiphyses removed. Bone cavity was washed three times by flushing with α-MEM medium (Wako) with a 25-G syringe. Bones were minced into chips and digested in 3 ml of α-MEM containing 10% (vol/vol) fetal bovine serum (FBS) in the presence of 1 mg/ml (wt/vol) of collagenase II (Gibco) for 1 h in a shaking incubator at 37 °C with a shaking speed of 200 rpm. After digestion, chips were washed again and incubated at 37 °C in a 5% CO_2 incubator and cultured for 3 days. On the third day of culture, the medium was changed to remove non-adherent cells and tissue debris and replaced with 6 ml of α-MEM containing 10% (vol/vol) FBS. After 5 days in culture, adherent cells were harvested with trypsin/0.02% (wt/vol) EDTA and passaged at a split ratio of 1:3. For osteogenic differentiation of MSCs, passage 4 cells were seeded at a density of 1×10^4 cells per well in a 24-well plate with α-MEM supplemented with 10% (vol/vol) FBS, 10^{-7} M dexamethasone, 10 mM B-glycerol phosphate and 50 ml ascorbate-2-phosphate in a total volume of 500 ml for 14 days. Alizarin red staining was performed using Calcified nodule Staining kit (Cell Biolabs, Inc).

Quantitative real-time reverse transcriptase polymerase chain reaction (qRT-PCR)

Total RNA was extracted using the RNeasy Mini kit (Qiagen). For complementary DNA synthesis, 0.5 µg RNA was reverse transcribed using random hexamer primers (Promega) and ImPromII reverse transcriptase (Promega). RT-PCR was performed using a Thermal Cycler Dice Real Time System II (Takara). Signals were detected using SYBR Premix Ex TaqII (Takara) with gene-specific primers (Supplementary Table S1). Relative

mRNA expressions of each targeted gene were expressed as the Ct value of each gene normalized to the Ct value of GAPDH using the ΔΔCt method.

Statistics

All statistical analyses of data were performed using JMP Pro 16.0 statistical software (SAS Institute Inc., Cary, NC, USA). All data are presented as means ± standard deviation. Significant differences between groups compared using unpaired *t*-tests. Significance was accepted at the level of $p < 0.05$.

Data availability

Data is provided within the manuscript or supplementary information files.

Received: 11 December 2023; Accepted: 8 October 2024
Published online: 22 October 2024

References

1. Otsuki, D. et al. Costal cartilage transplantation for treatment of growth plate injury in a rabbit model. *J. Child. Orthop.* **11**, 20–27. https://doi.org/10.1302/1863-2548-11-160209 (2017).
2. Shaw, N. et al. Regenerative medicine approaches for the treatment of pediatric physeal injuries. *Tissue Eng. Part. B Rev.* **24**, 85–97. https://doi.org/10.1089/ten.TEB.2017.0274 (2018).
3. Long, F. & Ornitz, D. M. Development of the endochondral skeleton. *Cold Spring Harb. Perspect. Biol.* **5**, a008334. https://doi.org/10.1101/cshperspect.a008334 (2013).
4. Hasler, C. C. & Foster, B. K. Secondary tethers after physeal bar resection: a common source of failure? *Clin. Orthop. Relat. Res.* 242–249. https://doi.org/10.1097/00003086-200212000-00031 (2002).
5. Joutoku, Z. et al. CCL21/CCR7 axis regulating juvenile cartilage repair can enhance cartilage healing in adults. *Sci. Rep.* **9**, 5165. https://doi.org/10.1038/s41598-019-41621-3 (2019).
6. Sambamurthy, N. et al. Chemokine receptor-7 (CCR7) deficiency leads to delayed development of joint damage and functional deficits in a murine model of osteoarthritis. *J. Orthop. Res.* **36**, 864–875. https://doi.org/10.1002/jor.23671 (2018).
7. Chi, B. J., Du, C. L., Fu, Y. F., Zhang, Y. N. & Wang, R. W. Silencing of CCR7 inhibits the growth, invasion and migration of prostate cancer cells induced by VEGFC. *Int. J. Clin. Exp. Pathol.* **8**, 12533–12540 (2015).
8. Liu, F. Y. et al. CCR7 regulates cell migration and invasion through JAK2/STAT3 in metastatic squamous cell carcinoma of the head and neck. *Biomed. Res. Int.* **2014**, 415375. https://doi.org/10.1155/2014/415375 (2014).
9. Yan, C. et al. Expression of vascular endothelial growth factor C and chemokine receptor CCR7 in gastric carcinoma and their values in predicting lymph node metastasis. *World J. Gastroenterol.* **10**, 783–790. https://doi.org/10.3748/wjg.v10.i6.783 (2004).
10. Günther, K. et al. Prediction of lymph node metastasis in colorectal carcinoma by expressionof chemokine receptor CCR7. *Int. J. Cancer.* **116**, 726–733. https://doi.org/10.1002/ijc.21123 (2005).
11. Yu, S. et al. A critical role of CCR7 in invasiveness and metastasis of SW620 colon cancer cell in vitro and in vivo. *Cancer Biol. Ther.* **7**, 1037–1043. https://doi.org/10.4161/cbt.7.7.6065 (2008).
12. Takeuchi, H. et al. CCL21 chemokine regulates chemokine receptor CCR7 bearing malignant melanoma cells. *Clin. Cancer Res.* **10**, 2351–2358. https://doi.org/10.1158/1078-0432.ccr-03-0195 (2004).
13. Mashino, K. et al. Expression of chemokine receptor CCR7 is associated with lymph node metastasis of gastric carcinoma. *Cancer Res.* **62**, 2937–2941 (2002).
14. Riol-Blanco, L. et al. The chemokine receptor CCR7 activates in dendritic cells two signaling modules that independently regulate chemotaxis and migratory speed. *J. Immunol.* **174**, 4070–4080. https://doi.org/10.4049/jimmunol.174.7.4070 (2005).
15. Yuan, L. H., Chen, X. L., Di, Y. & Liu, M. L. CCR7/p-ERK1/2/VEGF signaling promotes retinal neovascularization in a mouse model of oxygen-induced retinopathy. *Int. J. Ophthalmol.* **10**, 862–869. https://doi.org/10.18240/ijo.2017.06.06 (2017).
16. Cai, Q. Y. et al. CCR7 enhances the angiogenic capacity of esophageal squamous carcinoma cells in vitro via activation of the NF-κB/VEGF signaling pathway. *Am. J. Transl. Res.* **9**, 3282–3292 (2017).
17. Carlevaro, M. F., Cermelli, S., Cancedda, R. & Descalzi Cancedda, F. Vascular endothelial growth factor (VEGF) in cartilage neovascularization and chondrocyte differentiation: auto-paracrine role during endochondral bone formation. *J. Cell. Sci.* **113** (Pt 1), 59–69. https://doi.org/10.1242/jcs.113.1.59 (2000).
18. Chung, R., Foster, B. K. & Xian, C. J. The potential role of VEGF-induced vascularisation in the bony repair of injured growth plate cartilage. *J. Endocrinol.* **221**, 63–75. https://doi.org/10.1530/JOE-13-0539 (2014).
19. Erickson, C. B. et al. Anti-VEGF antibody delivered locally reduces bony bar formation following physeal injury in rats. *J. Orthop. Res.* **39**, 1658–1668. https://doi.org/10.1002/jor.24907 (2021).
20. Hosokawa, Y. et al. Depletion of b-series ganglioside prevents limb length discrepancy after growth plate injury. *BMC Musculoskelet. Disord.* **25**, 565. https://doi.org/10.1186/s12891-024-07704-7 (2024).
21. Zhu, H. et al. A protocol for isolation and culture of mesenchymal stem cells from mouse compact bone. *Nat. Protoc.* **5**, 550–560. https://doi.org/10.1038/nprot.2009.238 (2010).
22. Matsuoka, M. et al. Depletion of gangliosides enhances articular cartilage repair in mice. *Sci. Rep.* **7**, 43729. https://doi.org/10.1038/srep43729 (2017).

Author contributions

Conceptualization, M.M.; methodology, M.M., T.O., W.K. and Y.S.; software, M.M., Y.H., W.K. and Y.S.; validation, M.M., W.K. and Y.S.; formal analysis, M.M., W.K. and Y.S.; investigation, M.M., W.K. and Y.S.; resources, M.M., T.O., R.F., W.K., and Y.S.; data curation, M.M., T.O., and Y.H.; writing—original draft preparation, W.K. and Y.S.; writing—review and editing, M.M., W.K. and Y.S.; visualization, M.M., W.K., R.F. and K.H.; supervision, M.M., T.O. and N.I.; project administration, M.M.; funding acquisition, M.M. and N.I. All authors have read and agreed to the published version of the manuscript.

Funding

This study was supported by Grants-in-Aid for Scientific Research (No. 20K18017) from the Ministry of Education, Science, and Culture of Japan (Tokyo, Japan).

Declarations

Competing interests
The authors declare no competing interests.

Additional information
Supplementary Information The online version contains supplementary material available at https://doi.org/10.1038/s41598-024-75877-1.

Correspondence and requests for materials should be addressed to M.M.

Reprints and permissions information is available at www.nature.com/reprints.

Publisher's note Springer Nature remains neutral with regard to jurisdictional claims in published maps and institutional affiliations.